applied sciences

MDPI

Article

Identifying Parkinson's Disease from Gait Biomechanics Using a Participant-Level Machine Learning Analysis Pipeline

Li Jin

AI Biomechanics Research Laboratory, Department of Kinesiology, San José State University, San José, CA 95192, USA; li.jin@sjsu.edu

Abstract

Parkinson's disease (PD) is a progressive neurodegenerative disorder characterized by motor control, balance, and gait impairments that significantly elevate fall risk. Traditional gait analysis focuses on spatiotemporal parameters, while gait variability, asymmetry, and balance measures offer more sensitive indicators of PD-related motor deficits. Machine learning studies using wearable gait data frequently report high classification accuracy but lack biomechanical interpretability and methodological rigor. Using the PhysioNet Gait in Parkinson's Disease database, 93 individuals with PD and 72 healthy controls were analyzed during level-ground walking. Key biomechanical differences were identified: stride time coefficient of variation was significantly higher in PD bilaterally (left $p = 0.001$; right $p = 0.003$); swing-phase time was significantly reduced in both limbs (left $p = 0.003$; right $p = 0.001$); anterior–posterior center of pressure (COP) variability was significantly lower in PD for both limbs ($p < 0.001$); and COP path symmetry index was the most prominent asymmetry marker, significantly elevated in PD relative to controls ($p = 0.003$). A machine-learning analysis pipeline identified HistGradientBoosting as the best-performing classifier (AUC = 0.992; accuracy = 97.6%), but leave-one-study-out evaluation exposed substantial cross-protocol heterogeneity (AUC: 0.500–1.000), indicating that the model relied partly on dataset-specific patterns and may not generalize to independent acquisition protocols. Shapley Additive Explanations (SHAP) analysis showed classification was driven by a multimodal combination of clinical severity measures and biomechanical gait features rather than wearable metrics alone. A pre-specified gait-only sensitivity analysis that excluded clinical severity variables (UPDRS, UPDRSM, Hoehn and Yahr) confirmed that biomechanical features alone retained moderate, but substantially reduced, discriminative ability (gait-only holdout AUC = 0.844), supporting the interpretation that the headline performance reflects multimodal clinical separation rather than a stand-alone wearable-gait biomarker. These findings indicate that Parkinsonian gait impairment is characterized by timing instability and constrained forward COP progression. The combination of biomechanical analysis with interpretable predictive modeling represents a structured analysis pipeline for gait-based PD assessment; however, external validation in independent cohorts and prospective testing across acquisition protocols are required before such a pipeline can be deployed as a clinically generalizable digital biomarker.

Keywords: Parkinson's disease; gait biomechanics; center of pressure; wearable sensors; interpretable machine learning; digital biomarkers

Check for updates

Academic Editor: Stanislav Dadelo

Received: 19 April 2026
Revised: 14 June 2026
Accepted: 15 June 2026
Published: 23 June 2026

Copyright: © 2026 by the author. Licensee MDPI, Basel, Switzerland. This article is an open access article distributed under the terms and conditions of the Creative Commons Attribution (CC BY) license.

1. Introduction

Parkinson's disease (PD) is the second most prevalent neurodegenerative disease worldwide. The most recent Global Burden of Disease analysis estimated the global

prevalence of Parkinson's disease at approximately 11.77 million cases in 2021 [1]. The disease imposes a substantial and escalating public health burden: it was projected that global case numbers would increase by 112% from 2021 to about 25.2 million by 2050 [2]. PD is characterized by progressive loss of dopaminergic neurons in the substantia nigra pars compacta, disrupting the basal ganglia circuitry that regulates movement initiation, timing, and rhythmicity [3]. The resulting motor syndrome encompasses bradykinesia, muscular rigidity, resting tremor, and postural instability [3]. Among these manifestations, gait impairment stands out as a primary clinical concern, given both its prevalence and the intricate biomechanical deficits it embodies.

Gait disturbance represents one of the most disabling and clinically significant motor manifestations of Parkinson's disease, affecting the majority of patients across all stages of disease progression [4]. The PD gait pattern is characterized by reduced walking speed, shortened stride length, prolonged double-limb support time—collectively reflecting impaired central motor control, altered musculoskeletal movement mechanics and compromised dynamic balance [5,6]. Additionally, stride-to-stride temporal variability is recognized as a sensitive indicator of basal ganglia dysfunction. Elevated stride time variability reflects impaired rhythmic output from internal timing mechanisms and progressively worsens with disease severity [7]. Collectively, these features reflect a multidimensional impairment profile beyond what standard spatiotemporal parameters alone can capture.

The clinical significance of Parkinsonian gait impairment is underscored by its strong association with falls. Around 60–70% of PD patients were affected by fall incidents, and it was reported as a leading cause of injury and functional deterioration [8]. The general spatiotemporal values change, such as reduced cadence, shorter stride length, as well as greater mediolateral head and trunk displacement, were regarded as potential fall risk factors in PD gait [9]. Additionally, gait variability outcomes seem to be more sensitive to detecting fall risk [10,11]. This indicates that gait dynamic variables may yield more clinically informative biomarkers.

The foot-ankle kinetic outcome measurements offer an additional perspective for evaluating Parkinsonian gait. Center of pressure (COP) trajectories and variability reflect movement mechanics and balance control strategies during stance-phase, while temporal parameters such as stride time and stance time capture rhythmic inter-limb coordination. Bilateral gait coordination in PD is disrupted by asymmetric dopaminergic degeneration [12]. Gait asymmetry is recognized as one of three independent domains of Parkinsonian gait, and quantifying inter-limb differences across multiple outcome domains provides a more comprehensive characterization of disease-related motor dysfunction than single-parameter approaches [13,14]. Accordingly, inter-limb symmetry was evaluated across four complementary domains in the present study: mean stride time, reflecting asymmetric locomotor timing; mean stance time, capturing lateralized weight-bearing duration; peak vertical ground reaction force, indexing mechanical loading asymmetry between limbs; and COP path length, integrating the full spatial trajectory of weight transfer during stance, providing sensitivity to asymmetric propulsive and balance control deficits not captured by conventional spatiotemporal measures [12–15].

The instrumented wearable sensors, such as in-shoe force sensors and inertial measurement units (IMUs), have been widely used in gait assessment in both research and clinical settings [16]. The systems enable large-scale data collection and support the derivation of various biomechanical features in different locomotion tasks. The PhysioNet Gait in Parkinson's Disease database exemplifies this approach, providing multi-session, instrumented insole measurements from individuals with PD and healthy controls across different study

protocols and walking conditions, and has become a widely used benchmark for gait-based PD research [17].

Numerous machine learning studies have examined gait datasets derived from wearable sensors and reported high classification performance, with area under the receiver operating characteristic curve (AUC) values exceeding 0.95 using algorithms such as support vector machines, random forests, and gradient boosting classifiers [18–20]. However, several persistent methodological concerns limit the translational and scientific value of these findings. A predominant limitation among published studies is the aggregation of observations at the stride or session level without enforcing participant-level separation during training-test partitioning, which risks performance inflation due to data leakage [21]. Additionally, an overreliance on overall classification accuracy obscures how well models generalize across heterogeneous data collection protocols—a critical gap given the multi-study structure of the PhysioNet dataset and the goal of clinical deployment. Moreover, most published models operate as black boxes, offering little insight into which biomechanical features drive their predictions or how these relate to established pathophysiological mechanisms [22]. Beyond gait, machine learning has also been applied to a range of complementary motor-behavior signals for PD detection, including handwriting kinematics, speech and voice features, and upper-limb movement signatures captured from wearable inertial sensors and smartphone-based assessments [23,24]; collectively, these efforts indicate that no single modality alone resolves the heterogeneity of Parkinsonian motor expression, motivating the present focus on interpretable, biomechanically grounded gait-based modeling as one component of this broader landscape.

Explainable machine learning approaches, such as Shapley Additive Explanations (SHAP), offer a principled, game-theoretic framework for decomposing individual model predictions into quantified feature contributions [25]. When applied to gait classification pipelines, SHAP analysis can identify which biomechanical variables drive discrimination between PD and control groups, thereby grounding computational findings in interpretable biomechanical constructs. The combination of participant-level cross-protocol validation and SHAP-based explainability addresses the most critical methodological deficiencies in the existing PD gait machine learning studies.

The current study aimed to address the gaps using the PhysioNet Gait in Parkinson's Disease database. Specifically, we plan to: (1) quantify group differences across spatiotemporal and kinetic domains using participant-level statistical inference; (2) develop and evaluate a machine learning classification pipeline employing strict participant-wise data partitioning and leave-one-study-out cross-protocol evaluation; (3) apply SHAP-based feature analysis to identify the biomechanical and clinical drivers of model classification, linking computational outputs to interpretable pathophysiological mechanisms. Together, these objectives describe a structured, interpretable analysis pipeline intended to inform future digital gait biomarker development in PD, while explicitly acknowledging that external validation across cohorts and acquisition protocols will be required before this pipeline can be considered a fully established framework.

2. Materials and Methods

2.1. Dataset Structure and Study Protocol

This research investigated the publicly available Gait in Parkinson's Disease (PD) dataset [17]. The dataset uses the naming convention "Ga" (cognitive motor dual-task walking) [26], "Ju" (impact of rhythmic auditory stimulation) [27], and "Si" (treadmill walking) [28] to denote different data groups. The analysis includes 93 PD subjects (58 Male, 35 Female; 66.301 $\pm$ 9.500 years; 1.674 $\pm$ 0.086 m; 72.396 $\pm$ 11.960 kg), and 72 healthy control subjects (40 Male, 32 Female; 63.681 $\pm$ 8.700 years; 1.683 $\pm$ 0.086 m; 72.690 $\pm$ 12.418 kg). All

subjects walked on level ground at self-selected speeds for about two minutes [17]. All data processing, gait biomechanics variables calculation, feature extraction and machine learning algorithms evaluation were implemented in Python (v3.12) using Google Colaboratory (Google LLC, Mountain View, CA, USA).

Each subject wore an instrumented in-shoe system (Ultraflex Computer Dyno Graphy, Infotronic Inc., Tubbergen, The Netherlands) containing eight force sensors under each foot, sampled at 100 Hz [17]. The sensor placement can be found in the previous studies [17–19], and it is illustrated in Figure 1. The dataset provides 19 parameters per time-step: (1) time (seconds); (2) 16 individual vertical ground reaction force (VGRF) sensor values (8 per foot); and (3) 2 signals representing the summed total force for each foot [17]. Valid gait trials were identified using standardized filename patterns (e.g., GaCo01_01.txt). Recordings with corrupted column structures or prolonged zero-force segments were excluded prior to analysis.

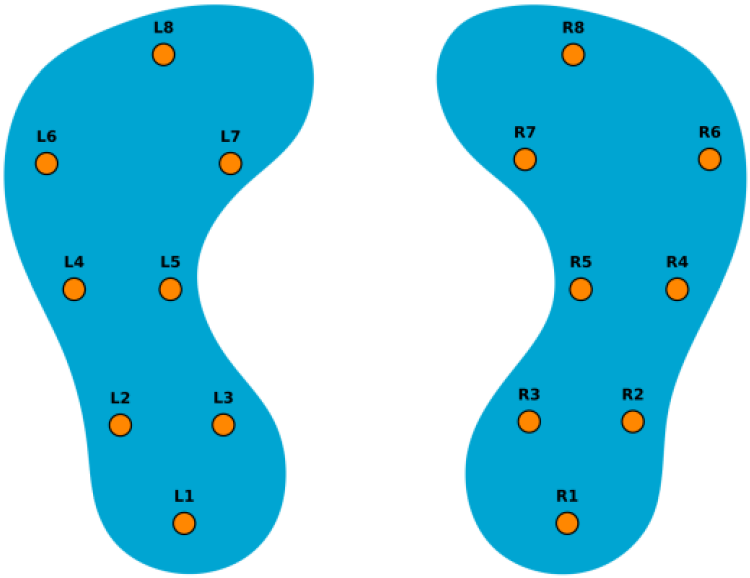


Figure 1. Schematic of the eight-sensor in-shoe Ultraflex Computer Dyno Graphy system used in the PhysioNet Gait in PD database [17]. Sensors L1–L8 (left foot) and R1–R8 (right foot) are positioned beneath standardized plantar anatomical landmarks, and they were highlighted in orange color (heel, lateral and medial rearfoot, lateral and central midfoot, lateral and medial metatarsal head regions, and hallux) [17,26–28]. Each sensor samples plantar vertical ground reaction force at 100 Hz with linearity within approximately ±7% of the calibrated load [17].

2.2. Gait Event Identification and Spatiotemporal Feature Extraction

Gait event detection was performed independently for each limb using the force-threshold method [29]. Stance-phase was defined as a continuous interval during which the total VGRF exceeded a threshold of 20 N [29]. Heel strike was identified as upward crossings of the threshold.

Stride time was calculated as the interval between consecutive heel-strikes of the same limb [28,30–34]. Stance duration was the time from threshold onset to offset, and swing duration was computed as the difference between stride and stance times [28,30–34]. Stride-to-stride temporal variability was quantified using the coefficient of variation (CV) of stride time for each limb, computed using its standard definition as the within-trial standard deviation of stride time divided by the corresponding within-trial mean stride time. As CV is a widely used and conventionally defined measure, an explicit equation is not reproduced here.

2.3. Gait Kinetic Variables from VGRF

Peak vertical ground reaction force (VGRF) was identified as the maximum force recorded during each stance phase. Stance-phase impulse was calculated as the time integral of the VGRF signal using the trapezoidal numerical integration method:

$$Impulse = \int_0^T F(t)dt \quad (1)$$

where T represents the stance-phase duration, and F refers to VGRF.

The loading rate was computed as the average slope of the VGRF curve between 20% and 80% of peak force within each stance phase.

2.4. Center of Pressure (COP) Calculation and the Plantar Loading Distribution

Center of pressure (COP) trajectories were estimated using a force-weighted average of the discrete sensor positions [35]:

$$COP_x(t) = \frac{\sum_{i=1}^{8} F_i(t) \cdot x_i}{\sum_{i=1}^{8} F_i(t)}, COP_y(t) = \frac{\sum_{i=1}^{8} F_i(t) \cdot y_i}{\sum_{i=1}^{8} F_i(t)} \quad (2)$$

where $F_i(t)$ is the force at sensor i, and x_i, y_i are its spatial coordinates in meters. COP path length was computed as the cumulative Euclidean distance traveled by the COP across stance time. COP dispersion was computed separately in the mediolateral (ML) and anteroposterior (AP) directions as the standard deviation of COP position along each axis during stance.

To characterize plantar loading distribution, forefoot-to-rearfoot loading ratios were also computed for each foot. Sensors were classified as forefoot vs. rearfoot based on their anteroposterior coordinate (positive vs. negative y in the local coordinate system). At each time point, forces under the forefoot sensors and rearfoot sensors were summed; the trial-level fore/rear ratio was then computed as the mean of the instantaneous ratios (with a small epsilon added in the denominator to avoid division by zero).

2.5. Inter-Limb Symmetry Indices

Inter-limb coordination was quantified using a normalized Symmetry Index (SI) [36–38]:

$$SI = \frac{100 \times |L - R|}{0.5 \times (L + R)} \quad (3)$$

where L and R represent the values for the left and right limbs, respectively. SI values were computed for mean stride time, mean stance time, peak force, and COP path length, yielding a dimensionless percentage measure where larger values indicate greater asymmetry.

2.6. Group Comparisons Statistical Analysis

Group differences between PD and control groups were evaluated for each participant-level outcome using Welch's two-sample *t*-test (two-sided). Welch's test was selected because it does not assume equal variances between groups. Mean differences were calculated as PD minus Control, and 95% confidence intervals were estimated using Welch's approximation.

To account for multiple comparisons across biomechanical outcomes, false discovery rate (FDR) control was applied using the Benjamini–Hochberg procedure. Statistical significance was defined as FDR-adjusted q-values < 0.05. Standardized effect sizes were calculated using Hedges' g, which incorporates a small-sample correction to Cohen's d and is appropriate for group comparisons with unequal sample sizes. The magnitude of effect

sizes was interpreted using conventional thresholds, where $|g| \approx 0.2$ indicates a small effect, $|g| \approx 0.5$ a moderate effect, and $|g| \geq 0.8$ a large effect.

2.7. Waveform Analysis and Statistical Parametric Mapping

To evaluate continuous stance-phase kinetics, stance intervals were identified and vertical ground reaction force (VGRF) waveforms were time-normalized to 101 points representing 0–100% of the stance-phase. Within each recording session, stance-phase waveforms were averaged across strides to obtain a single trial-level mean waveform per limb. Group differences in waveform shape across the stance continuum were assessed using a two-sample Statistical Parametric Mapping (SPM) *t*-test with random field theory-based inference at $\alpha = 0.05$ [39].

2.8. Machine Learning Model Exploration

A participant-level machine learning pipeline was implemented to classify PD versus control using an aggregated feature matrix. Candidate models included Random Forest (600 trees; class-weight balanced) [40], Histogram Gradient Boosting [41,42], support vector machine with a radial basis function kernel (SVM-RBF) [43], and a multilayer perceptron (MLP) [44], implemented using scikit-learn [45]. A participant-wise holdout split (25%) was generated using a grouped random sampling strategy (implemented via GroupShuffleSplit in scikit-learn), with participant ID as the grouping variable, ensuring that all observations from a given participant were assigned exclusively to either the training or testing set.

To clarify how repeated measures were handled, gait features were first computed at the trial level, yielding one feature vector per valid recording session and were then aggregated to one observation per participant by averaging across all valid trials of the same participant. Within each trial-level and participant-level feature vector, left- and right-limb features were retained as separate, side-specific columns rather than averaged across limbs (e.g., StrideL_CV and StrideR_CV; COP_AP_SD_L and COP_AP_SD_R; ForeRearRatio_L and ForeRearRatio_R), preserving any limb-specific information that could carry asymmetry-related discriminative signal; inter-limb symmetry indices (SI) were computed as separate scalar features as described in Section 2.5. The number of recording sessions varied between 1 and 2 per participant depending on the source protocol (Ga, Ju, Si). The final feature matrix used for classification therefore contained one row per participant, ensuring strict statistical independence between observations and eliminating any possibility of within-subject information leakage between training and testing partitions. A participant-wise 75%/25% holdout split was generated using participant ID as the grouping variable, ensuring that all data from a given participant were assigned exclusively to either the training or testing set. All preprocessing steps that depend on the data distribution, including median imputation of missing values and model-specific standardization where applicable, were fitted exclusively within the corresponding training fold during cross-validation or within the full training split during final holdout evaluation and were then applied to the corresponding validation or held-out test data within a scikit-learn Pipeline object. Missing clinical severity values (UPDRS total available for 91 of 93 PD participants; UPDRSM available for the same 91 of 93 PD participants) and Hoehn and Yahr values, where present in the source data, were handled by this same training-fold median imputation strategy rather than by case-wise exclusion, so that no participants were dropped from the analysis on the basis of missing clinical scores; imputation parameters were derived only from the training data within each fold or training split to preserve the integrity of the cross-validation and holdout evaluation procedure. No target-based feature selection, target-based filtering, or hyperparameter tuning step used information from the held-out data. The full classification workflow, including data partitioning, preprocess-

ing, model selection, leave-one-study-out evaluation, and SHAP-based interpretation, is summarized schematically in Figure 2.

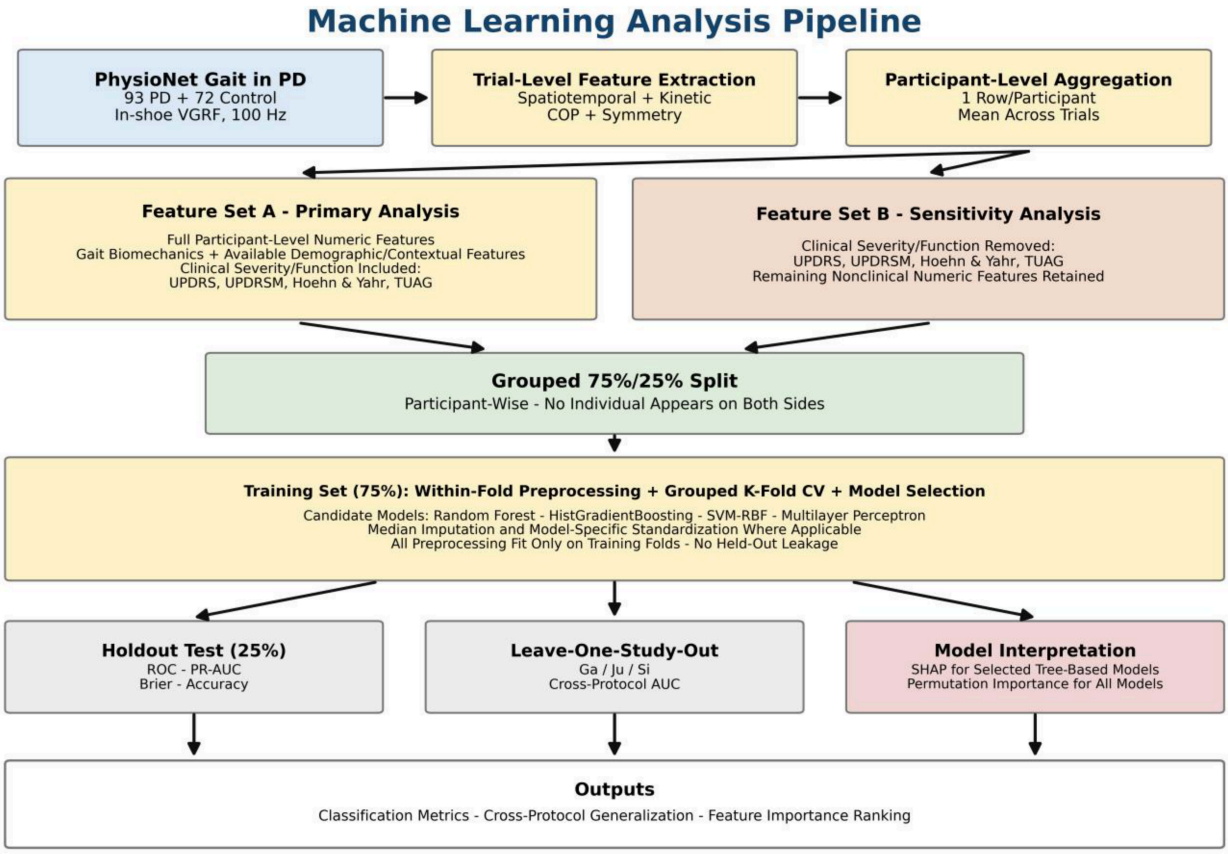


Figure 2. Schematic overview of the machine learning analysis pipeline. Trial-level gait features were extracted from the in-shoe vertical ground reaction force signals and aggregated to one observation per participant by averaging across all valid recordings from the same participant. Left- and right-limb features were retained as separate side-specific columns, and inter-limb symmetry indices were included as separate scalar features. The participant-level feature matrix was evaluated using two parallel feature sets: a primary analysis feature set containing the full participant-level numeric feature matrix, including gait biomechanics, available demographic/contextual variables, clinical severity variables, and the TUAG functional mobility score; and a sensitivity analysis feature set in which clinical severity variables and the TUAG score were removed. A participant-wise 75%/25% grouped holdout split was applied using participant ID as the grouping variable, ensuring that all observations from a given individual remained on only one side of the split. Within grouped cross-validation on the training set, preprocessing steps, including median imputation and model-specific standardization where applicable, were fitted only on the corresponding training folds and then applied to the validation folds. For final holdout evaluation, the same preprocessing pipeline was fitted on the full training split and then applied to the participant-wise held-out test set. Final model performance was evaluated on the participant-wise held-out test set and through leave-one-study-out cross-protocol evaluation across the Ga, Ju, and Si subsets. Model interpretation was performed using permutation importance on the held-out test set, with SHAP additionally applied when the selected model was tree-based.

Within the training set, grouped cross-validation (by participant ID) was used to evaluate candidate models, and the model achieving the highest mean area under the receiver operating characteristic curve (AUC) was selected. Final model performance was assessed on the held-out test set using ROC analysis, precision–recall analysis, confusion matrix–derived metrics, and the Brier score to evaluate probabilistic calibration.

To assess generalizability across protocol heterogeneity, a leave-one-study-out analysis was performed. For each protocol subset (Ga, Ju, Si), all participants from that subset were held out as the test set while the model was trained on the remaining data. Because this analysis evaluates transportability across protocol-defined cohorts, its results were interpreted separately from the primary participant-wise holdout evaluation.

Model explainability was assessed using SHAP values [25] for the selected tree-based model, complemented by permutation importance computed on the holdout set. SHAP analysis summary plots were used to rank features according to their contributions to model predictions. Because the feature matrix included both gait-derived biomechanical features and clinical/demographic variables (when available), feature importance rankings were interpreted as reflecting a combination of biomechanical and non-biomechanical contributors to classification.

2.9. Gait-Only Sensitivity Analysis

To explicitly evaluate the contribution of biomechanical gait features in the absence of clinical severity information, a pre-specified gait-only sensitivity analysis was conducted that mirrors the primary classification pipeline described in Section 2.8 with one modification: all clinical severity variables (UPDRS total, UPDRSM, and Hoehn and Yahr stage) and the Timed Up and Go (TUAG) functional mobility score were removed from the feature matrix prior to the participant-wise 75%/25% group split. All other elements of the pipeline were held identical to the primary analysis, including participant-level aggregation, separate retention of left and right limb features, the grouped 75%/25% holdout split, the candidate model set (Histogram Gradient Boosting, Random Forest, SVM-RBF, multilayer perceptron), grouped cross-validation on the training fold, within-fold median imputation and model-specific standardization where applicable, the held-out test-set evaluation (ROC, PR, accuracy, Brier), and the leave-one-study-out cross-protocol evaluation. Model interpretation was repeated for the best-performing gait-only model using permutation importance on the held-out test set, with SHAP analysis additionally applied when the selected model was tree-based. This analysis directly addresses the question of whether the participant-level gait biomechanics derived from the in-shoe sensors are, on their own, capable of separating PD and control participants in this dataset, independent of clinical severity covariance.

3. Results

3.1. Participant Characteristics

The final analytic sample comprised 93 participants with PD and 72 healthy controls. Participant-level demographics extracted from the dataset indicated that the PD group was modestly older than the control group, but this difference did not meet conventional statistical significance (Table 1, PD: 66.301 $\pm$ 9.500 years; Control: 63.681 $\pm$ 8.700 years; Welch $p = 0.067$). Sex distribution was similar between groups (PD: 58 male/35 female; Control: 40 male/32 female; chi-square $\chi^2 = 0.780$, $p = 0.377$). Height (PD 1.674 $\pm$ 0.086 m; Control 1.683 $\pm$ 0.086 m, Welch $p = 0.554$) and weight (PD: 72.396 $\pm$ 11.960 kg; Control 72.690 $\pm$ 12.418 kg, Welch $p = 0.879$) were also similar. In the PD group, Hoehn and Yahr stage ranged from 2.0 to 3.0 with a mean of 2.258 $\pm$ 0.343 (Table 1) and a distribution of stage 2.0 ($n = 55$), stage 2.5 ($n = 28$), stage 3.0 ($n = 10$). The Unified Parkinson's Disease Rating Scale (UPDRS) total scores (available for 91/93 PD participants) spanned 13–70 (mean 31.615 $\pm$ 11.825), and the Unified Parkinson's Disease Rating Scale motor section (UPDRSM) score averaged 19.318 $\pm$ 7.656, consistent with mild-to-moderate disease severity.

Table 1. Subject basic characteristics between Parkinson's Disease (PD) and Control Group (CG). Statistically significant differences between the two groups were highlighted in bold and denoted with an asterisk (*).

Variables	Subject Basic Characteristics for Parkinson's Disease (PD, n = 93) vs. Control Group (CG, n = 72), Mean (SD), Welch_p, False Discovery Rate (FDR)_q, Hedges'_g				
	PD	**CG**	**Welch_p**	**FDR_q**	**Hedges'_g**
Age	66.301 (9.500)	63.681 (8.700)	0.067	0.202	0.285
Height	1.674 (0.086)	1.683 (0.086)	0.554	0.831	−0.093
Weight	72.396 (11.960)	72.690 (12.418)	0.879	0.879	−0.024
Gender-Male	58	40			
Gender-Female	35	32			
Hoehn & Yahr	2.258 (0.343)				
UPDRS total	31.615 (11.825)				
UPDRSM	19.318 (7.656)				

These demographic patterns suggest that the observed gait differences are unlikely to be explained solely by age imbalance; however, given the modest age shift, age-related effects remain plausible as a partial contributor in multivariable classification models.

3.2. Spatiotemporal Gait Outcomes

In summary (Table 2), the most consequential spatiotemporal findings were the bilateral elevation of stride time variability (Hedges' $g \approx 0.468$–0.502, moderate effect) and the bilateral reduction in swing-phase time (Hedges' $|g| \approx 0.458$–0.539, moderate effect); other spatiotemporal parameters (mean stride time, cadence, stride-time symmetry) showed only small, non-significant differences. The most pronounced spatiotemporal differences were observed in stride-to-stride temporal variability. Stride time coefficient of variation was significantly higher in PD for both limbs (Table 2, Figure 3): left stride time coefficient of variation (StrideL_CV, Welch $p = 0.001$); right stride time coefficient of variation (StrideR_CV, Welch $p = 0.003$). Figure 3 illustrates the distributional separation for both the left and right-side stride time coefficient of variation, with the PD group showing higher central tendency and a wider dispersion.

Table 2. Kinematic output variables between Parkinson's Disease (PD) and Control Group (CG). Statistically significant differences between the two groups were highlighted in bold and denoted with an asterisk (*).

Kinematic Variables	Parkinson's Disease (PD, n = 93) vs. Control Group (CG, n = 72), Mean (SD), 95% Confidence Interval Difference (95% CI_Diff), Welch_p, False Discovery Rate (FDR)_q, Hedges'_g					
	PD	**CG**	**95%CI_Diff**	**Welch_p**	**FDR_q**	**Hedges'_g**
Cadence_SPM	112.015 (14.986)	111.455 (9.032)	[−3.161, 4.281]	0.767	0.797	0.044
Stride Time_L	1.096 (0.144)	1.088 (0.090)	[−0.028, 0.045]	0.637	0.781	0.070
Stride Time_R	1.078 (0.146)	1.068 (0.101)	[−0.028, 0.049]	0.586	0.753	0.081
StrideL_CV	0.199 (0.151)	0.131 (0.107)	[0.028, 0.107]	**0.001** *	**0.005** *	0.502
StrideR_CV	0.212 (0.168)	0.139 (0.137)	[0.026, 0.120]	**0.003** *	**0.008** *	0.468
StanceL	0.737 (0.118)	0.709 (0.067)	[−0.001, 0.057]	0.056	0.126	0.282
StanceR	0.730 (0.111)	0.694 (0.066)	[0.009, 0.064]	**0.010** *	**0.027** *	0.384
SwingL	0.357 (0.051)	0.378 (0.037)	[−0.035, −0.007]	**0.003** *	**0.008** *	−0.458
SwingR	0.347 (0.054)	0.374 (0.042)	[−0.042, −0.012]	**0.001** *	**0.003** *	−0.539
SI_Stride Time	5.268 (7.957)	3.485 (6.374)	[−0.420, 3.986]	0.112	0.215	0.243
SI_Stance Time	6.315 (6.622)	4.558 (6.543)	[−0.283, 3.797]	0.091	0.189	0.265

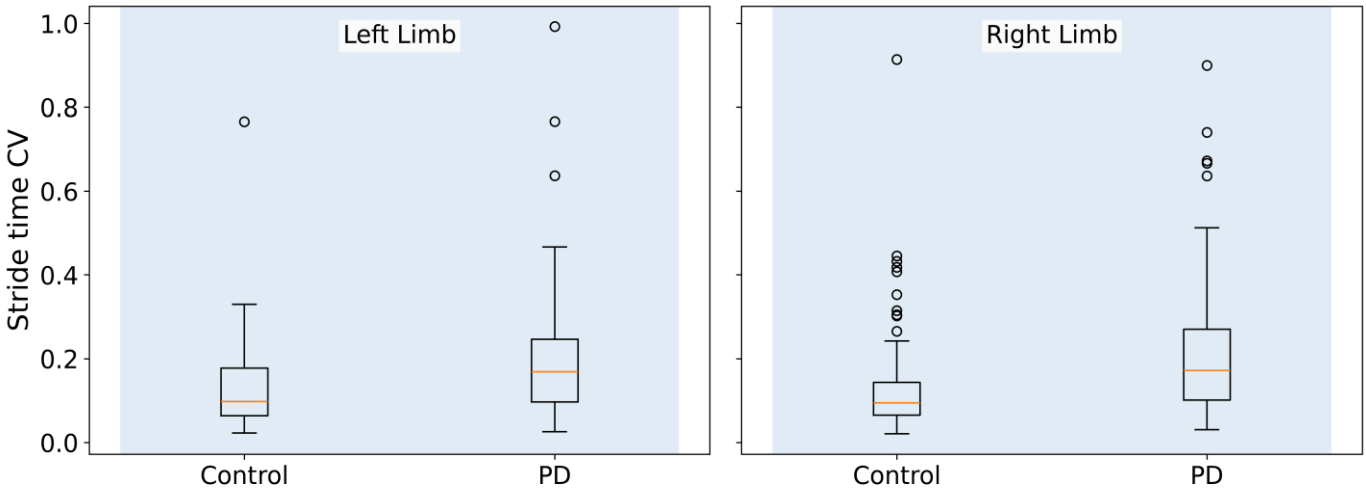


Figure 3. Stride time coefficient of variation between the control (n = 72) and Parkinson's Disease (PD) Group (n = 93). The shaded area highlights the significant difference between the comparisons.

Additionally, timing outcomes indicated phase redistribution within the gait cycle between the two groups. Specifically, swing-phase time was significantly shorter in the PD group for both the left (Welch p = 0.003) and the right limb (Welch p = 0.001) compared to the control group (Table 2), while right stance time (StanceR) was significantly longer than that of the control group (Welch p = 0.010). Together, these results suggest a shift toward relatively longer weight-bearing and shorter swing, consistent with cautious gait strategies and altered dynamic balance management.

3.3. Kinetic Outcome Variables from Force Measurement

Kinetic outcome variables are summarized in Table 3. Loading rate showed a nominal reduction in the PD group for the right limb (Welch p = 0.027), but it did not pass the FDR correction (FDR q = 0.066). Additionally, peak vertical force and stance-phase impulse did not differ significantly between the two groups.

Table 3. Kinetic output variables between Parkinson's Disease (PD) and Control Group (CG). Statistically significant differences between the two groups were highlighted in bold and denoted with an asterisk (*).

Kinetic Variables	Parkinson's Disease (PD, n = 93) vs. Control Group (CG, n = 72), Mean (SD), 95% Confidence Interval Difference (95% CI_Diff), Welch_p, False Discovery Rate (FDR)_q, Hedges'_g					
	PD	**CG**	**95%CI_Diff**	**Welch_p**	**FDR_q**	**Hedges'_g**
Peak_Force_L	1062.557 (173.082)	1090.951 (206.680)	[−88.219, 31.432]	0.350	0.543	−0.150
Peak_Force_R	1059.613 (169.460)	1078.840 (205.425)	[−78.383, 39.930]	0.521	0.704	−0.103
Impulse_L	493.559 (95.601)	487.474 (96.075)	[−23.647, 35.817]	0.687	0.787	0.063
Impulse_R	489.444 (85.063)	476.620 (101.210)	[−16.509, 42.157]	0.389	0.553	0.138
LoadingRate_L	7789.143 (4007.566)	8687.584 (3361.660)	[−2032.231, 235.348]	0.120	0.215	−0.239
LoadingRate_R	7487.435 (3542.645)	8728.396 (3533.648)	[−2338.038, −143.883]	0.027	0.066	−0.349
COP_Path_L	273.258 (61.718)	271.233 (59.808)	[−16.782, 20.831]	0.832	0.832	0.033
COP_Path_R	278.083 (60.060)	275.272 (60.667)	[−15.922, 21.544]	0.767	0.797	0.046
COP_ML_SD_L	0.033 (0.007)	0.035 (0.009)	[−0.004, 0.001]	0.194	0.327	−0.208
COP_ML_SD_R	0.035 (0.009)	0.034 (0.008)	[−0.002, 0.003]	0.700	0.787	0.060
COP_AP_SD_L	0.344 (0.037)	0.382 (0.028)	[−0.048, −0.028]	**<0.001** *	**<0.001** *	−1.120
COP_AP_SD_R	0.353 (0.036)	0.385 (0.029)	[−0.041, −0.021]	**<0.001** *	**<0.001** *	−0.940
ForeRearRatio_L	1.287 (0.586)	0.937 (0.301)	[0.210, 0.488]	**<0.001** *	**<0.001** *	0.720
ForeRearRatio_R	1.280 (0.590)	0.934 (0.247)	[0.212, 0.480]	**<0.001** *	**<0.001** *	0.730
SI_Peak Force	6.042 (5.743)	5.328 (4.293)	[−0.829, 2.257]	0.362	0.543	0.138
SI_COP_Path	6.117 (5.500)	3.997 (3.412)	[0.741, 3.498]	**0.003** *	**0.008** *	0.448

3.4. Center of Pressure (COP) Dynamics

In summary (Table 3), the largest kinetic effects were the bilateral reduction in anterior–posterior COP dispersion (Hedges' $|g| \approx 0.940$–1.120, large effect) and the bilateral elevation of the forefoot-to-rearfoot loading ratio (Hedges' $|g| \approx 0.720$–0.730, moderate-to-large effect); the COP path symmetry index also showed a moderate elevation in PD (Hedges' $|g| \approx 0.448$). Peak force, impulse, and loading rate showed only small, non-significant effects after FDR correction. Center of pressure (COP) derived metrics showed the strongest group differences observed in the participant-level feature set. Specifically, COP in anterior–posterior (AP) direction standard deviation dispersion (COP_AP_SD) was significantly reduced in the PD group for both limbs (Table 3, Figure 4): left side comparisons (Welch $p < 0.001$, FDR $q < 0.001$); right side comparisons (Welch $p < 0.001$, FDR $q < 0.001$). In contrast, COP in the medial-lateral direction standard deviation dispersion (COP_ML_SD) did not show a significant difference between the two groups for both limbs (Table 3).

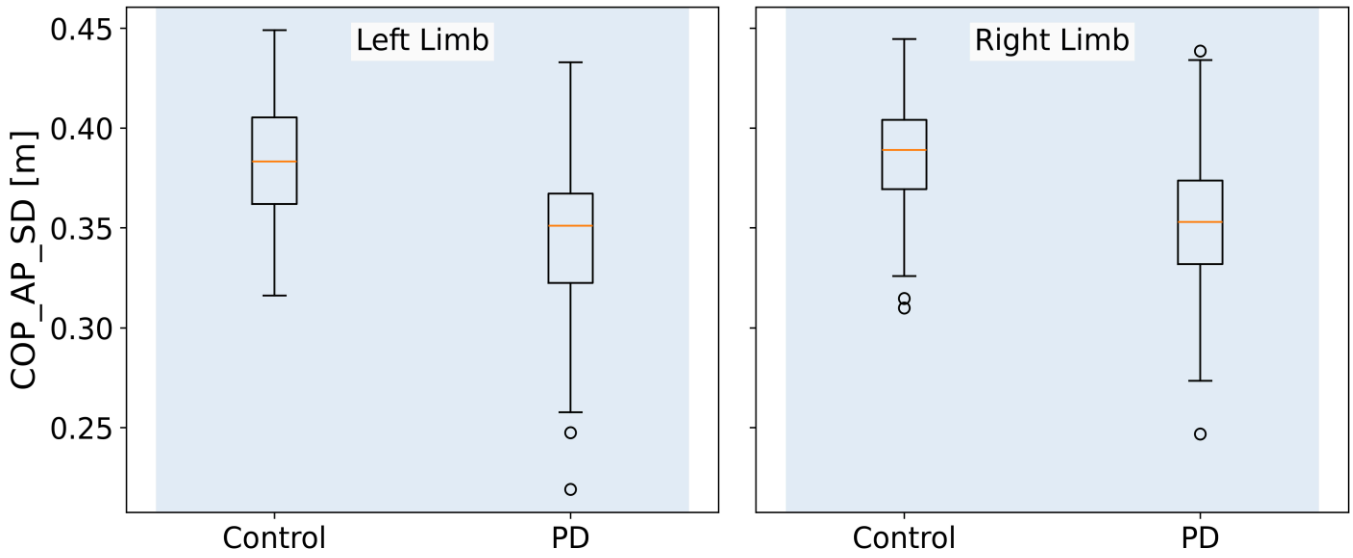


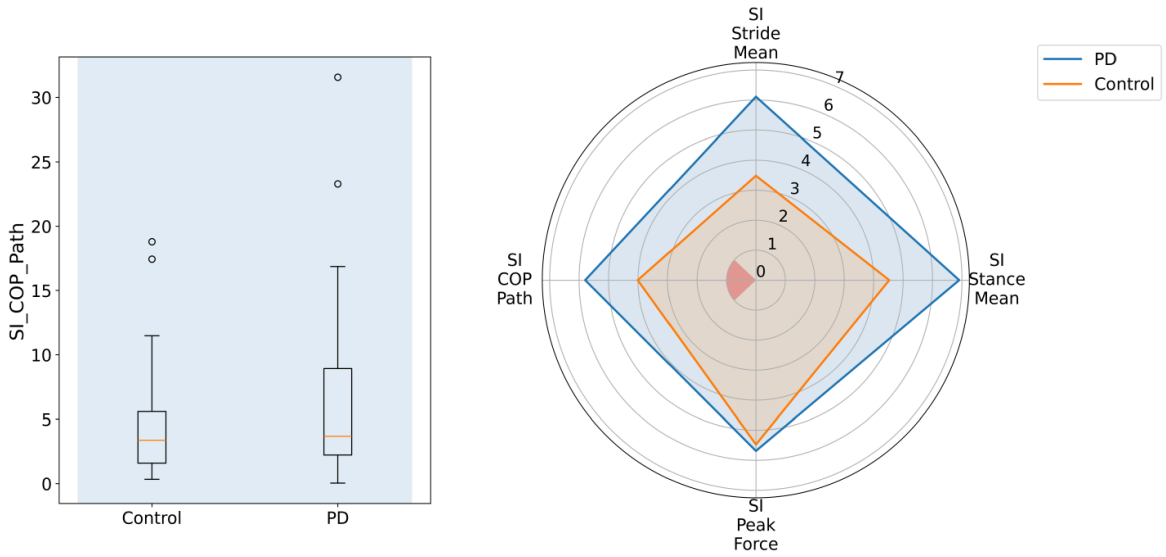
Figure 4. Center of pressure (COP) in anterior–posterior (AP) direction dispersion comparisons between the control ($n = 72$) and Parkinson's Disease (PD) Group ($n = 93$). The shaded area highlights the significant difference between the comparisons.

3.5. Plantar Loading Distribution

Plantar loading distribution differed significantly between groups. Forefoot-to-rearfoot ratios (ForeRearRatio) were higher in PD for both limbs (Table 3): ForeRearRatio_L and ForeRearRatio_R (Welch $p < 0.001$, FDR $q < 0.001$). This finding indicates a systematic shift in plantar loading distribution toward the forefoot in PD within the coordinate convention used in the in-shoe sensor system.

3.6. Inter-Limb Symmetry Analysis

Symmetry indices (SI) are summarized in Table 3 and Figure 5. The most significant asymmetry finding was the COP path symmetry index (SI_COP_Path) between the two groups: the PD group significantly increased the COP path symmetry index compared to the control group (Welch $p = 0.003$, FDR $q = 0.008$). Remaining symmetry indices showed smaller between-group differences that did not survive FDR correction, indicating that COP path asymmetry was the most discriminative asymmetry marker among those evaluated in this dataset.



(**a**) (**b**)

Figure 5. (**a**) Center of pressure (COP) path symmetry index (SI) comparisons between the control (n = 72) and Parkinson's Disease (PD) Group (n = 93); (**b**) Radar plot of symmetry index (SI) for mean stride time, mean stance time, peak force, and COP path length between the two groups. The orange shaded region indicates a statistically significant between group difference in SI_COP_Path.

3.7. Stance-Phase Waveform Analysis

Waveform-level analysis of stance-phase VGRF revealed statistically localized differences between PD and control groups (Figure 6). In the left limb, two significant clusters were identified in early stance (approximately 0–13% stance; cluster $p < 0.001$) and late stance (approximately 90–96% stance; cluster $p = 0.015$). In the right limb, four clusters were detected: a brief cluster at stance onset (approximately 0–1% stance; cluster $p = 0.050$), an early-stance cluster (approximately 6–12% stance; cluster $p = 0.015$), a mid-stance cluster (approximately 34–55% stance; cluster $p < 0.001$), and a late-stance cluster (approximately 90–94% stance; cluster $p = 0.033$). Overall, these findings indicate that PD-related waveform differences are concentrated in early and late stance, with additional mid-stance modulation observed in the right limb.

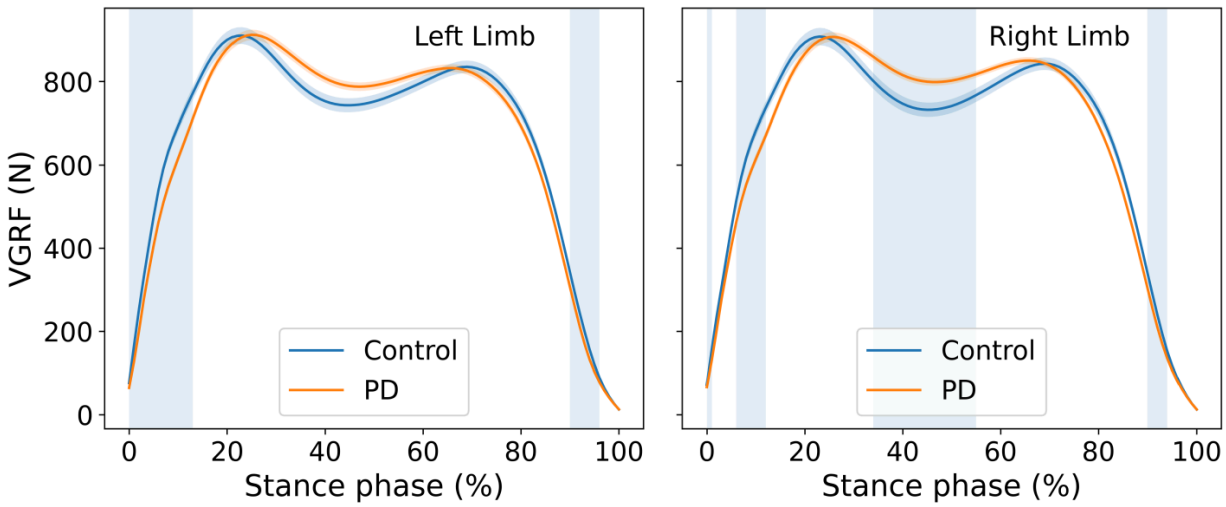


Figure 6. Time-normalized stance-phase vertical ground reaction force (VGRF) waveforms between the control (n = 72) and Parkinson's Disease (PD) Group (n = 93). The shaded area highlights the significant difference between the comparisons.

3.8. Machine Learning Classification

The machine-learning pipeline identified HistGradientBoosting as the best performing model. In grouped cross-validation on the training split, HistGradientBoosting achieved a mean area under the receiver operating characteristic curve (AUC) of 1.000 (SD = 0.000) and a mean Brier score of 0.017 (Table 4), outperforming Random Forest (AUC = 0.987), SVM-RBF (AUC = 0.980), and multilayer perceptron (AUC = 0.962). When evaluated on the participant-wise holdout test set, the selected model maintained very high performance, with an AUC of 0.992 and a Brier score of 0.025. The holdout set contained 42 participants (Control n = 14; PD n = 28), and classification accuracy remained high (accuracy = 0.976). Class-level metrics were similarly strong: Control precision/recall/F1 = 1.000/0.929/0.963, and PD precision/recall/F1 = 0.966/1.000/0.982. The average precision (PR AUC) was 0.996 (Table 4).

Table 4. Machine-learning benchmarking, final model performance, and protocol robustness for PD classification. Note: All four candidate models were benchmarked on the training split using grouped cross-validation (CV AUC and CV Brier reported as mean (SD)). For full transparency, each model was then evaluated on the participant-wise held-out test set (Holdout AUC, PR-AUC, Brier, Accuracy, Control F1, PD F1) and on the leave-one-study-out cross-protocol analysis (Protocol AUC for Ga, Ju, and Si). Final model selection was based exclusively on the highest mean grouped-CV AUC (HistGradientBoosting); the holdout and cross-protocol values for the non-selected models are reported for comparison only and were not used in the selection decision, preserving the integrity of the train/test partition. The selected model was highlighted in bold.

Model	Selected	CV AUC	CV Brier	Holdout AUC	PR-AUC	Accuracy	CG F1	PD F1	Protocol AUC (GA/JU/SI)
HistGradientBoosting	**Yes**	1.000 (0.000)	0.017 (0.018)	0.992	0.996	0.976	0.963	0.982	1.000/0.934/0.500
Random Forest	No	0.987 (0.008)	0.062 (0.010)	0.964	0.983	0.881	0.839	0.906	0.987/0.997/0.887
SVM (RBF Kernel)	No	0.980 (0.019)	0.053 (0.022)	0.926	0.967	0.833	0.774	0.868	0.900/0.500/0.962
Multiplayer Perceptron	No	0.962 (0.035)	0.069 (0.035)	0.929	0.967	0.810	0.750	0.846	1.000/0.746/0.908

Protocol-robustness analysis using leave-one-study-out evaluation revealed heterogeneous transportability across protocol-defined subsets. The model maintained strong discrimination when Ga was held out (AUC = 1.000) and when Ju was held out (AUC = 0.934), but performance dropped to AUC = 0.500 when Si was held out (Table 4). These results indicate that although the feature set is highly discriminative overall, model generalization across heterogeneous study protocols is not uniformly strong.

SHAP analysis was used to interpret the contribution of individual features to model predictions. The SHAP summary plot ranked variables according to their influence on the classifier output and showed that the strongest contributors were clinical severity measures, including UPDRS, UPDRSM, and Hoehn and Yahr stage (Figure 7). Among biomechanical variables derived from the wearable force-sensor data, the forefoot-to-rearfoot loading ratio, particularly the right-sided measure, emerged as the most influential gait-related feature. Additional contributors included walking speed, functional mobility measures such as the Timed Up and Go assessment (TUAG), and demographic or contextual variables including age and trial index. Several additional gait-derived metrics, including COP dispersion measures and stance-phase timing variables, contributed more modestly to the model output. Overall, the SHAP results indicate that classification performance was driven by a multimodal combination of clinical severity indicators and biomechanical gait features rather than by any single wearable sensor-derived variable. The biomechanical interpretation of the most influential gait-derived features is consistent with the group-comparison findings.

The elevated right-sided forefoot-to-rearfoot ratio reflects the anteriorly displaced plantar pressure distribution associated with the forward-flexed trunk posture characteristic of PD, while the COP dispersion features capture the constrained anteroposterior weight transfer during stance. Together, these top-ranked features describe a coherent profile of impaired forward propulsion and altered loading distribution, demonstrating that the model's selections align with established PD biomechanics.

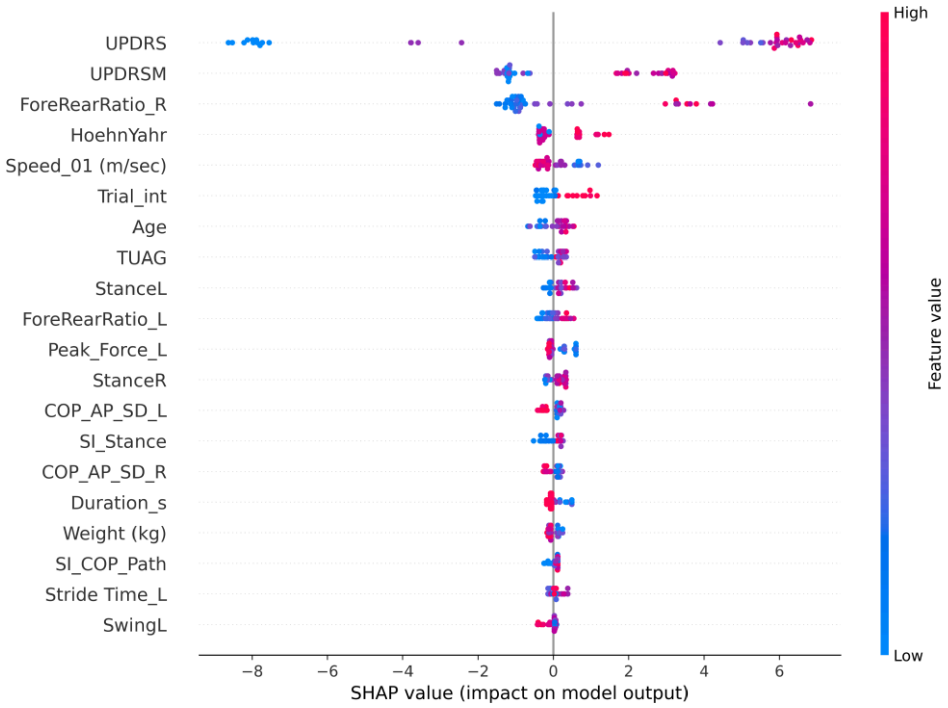


Figure 7. Shapley Additive Explanations (SHAP) summary plot feature contributions to the model predictions for the selected tree-based classifier.

Consequently, the high classification performance should be interpreted as reflecting multimodal separation between PD and control participants rather than evidence that gait-derived wearable metrics alone provide uniformly protocol-generalizable PD detection in this dataset.

3.9. Gait-Only Sensitivity Analysis Result

When clinical severity variables (UPDRS, UPDRSM, Hoehn and Yahr) and the TUAG functional mobility score were excluded prior to the participant-wise 75%/25% split (Section 2.9), the SVM with a radial basis function kernel emerged as the best-performing gait-only classifier on the basis of mean grouped-CV AUC (0.932 ± 0.038), supplanting HistGradientBoosting, which had been selected in the primary multimodal analysis. On the participant-wise holdout test set, the selected gait-only model achieved an AUC of 0.844, a Brier score of 0.182, an average precision (PR-AUC) of 0.933, and an overall accuracy of 0.738 (Table 5), substantially below the headline performance of the full multimodal model (AUC = 0.992; Brier = 0.025). Class-level F1 scores on the same holdout split were 0.621 (Control) and 0.800 (PD). On the leave-one-study-out cross-protocol evaluation, the gait-only model retained AUC = 0.845 when Ga was held out and AUC = 0.833 when Si was held out, but collapsed to near-chance performance (AUC = 0.500) when Ju was held out—a notable shift relative to the primary analysis, in which the Si treadmill subset rather than the Ju subset had been the failure point. This pattern shift suggests that the treadmill-specific failure of the primary multimodal model was driven in part by protocol-correlated heterogeneity in the clinical severity variables, whereas in their absence the dominant source of

cross-protocol failure becomes the Ju (rhythmic auditory stimulation) subset, consistent with auditory cueing acting to normalize PD-related timing variability and compress the gait-derived discriminative signal between groups. Permutation importance on the selected gait-only model identified bilateral anteroposterior COP dispersion (COP_AP_SD_L and COP_AP_SD_R), walking speed, and the COP path symmetry index (SI_COP_Path) as the principal biomechanical contributors, confirming that the residual gait-derived signal after removal of clinical severity features is dominated by AP COP and walking-speed features. Together, these results indicate that biomechanical gait features alone retain moderate, but substantially reduced, discriminative ability relative to the multimodal model, supporting the interpretation that the high headline AUC of the primary analysis is driven in large part by the inclusion of clinical severity variables rather than by the wearable-gait signal in isolation.

Table 5. Gait-only sensitivity analysis: classification performance and protocol robustness after removing clinical severity variables (UPDRS, UPDRSM, Hoehn and Yahr) and the TUAG score from the feature matrix. The selected model was highlighted in bold.

Model (Gait-Only)	Selected	CV AUC	Holdout AUC	Holdout Brier	Accuracy	CG F1	PD F1	Protocol AUC (Ga/Ju/Si)
HistGradientBoosting	No	0.899 (0.054)	0.773	0.227	0.738	0.686	0.776	0.761/0.890/0.827
Random Forest	No	0.903 (0.054)	0.814	0.174	0.762	0.643	0.821	0.879/0.941/0.794
SVM (RBF Kernel)	**Yes**	0.932 (0.038)	0.844	0.182	0.738	0.621	0.800	0.845/0.500/0.833
Multilayer Perceptron	No	0.924 (0.037)	0.834	0.200	0.786	0.690	0.836	0.891/0.500/0.833

4. Discussion

This study utilized a participant-level machine-learning analysis pipeline to characterize the biomechanical landscape of PD gait. Our findings indicate that PD gait impairment in this cohort is defined by elevated stride time variability, reduced swing time, altered plantar load distribution, constrained COP forward progression and elevated inter-limb asymmetry of COP path length, all observed in the absence of significant changes in mean cadence or stride time. This pattern is consistent with the "force-rhythm dichotomy" proposed previously [46]. This suggests that PD impairment reflects not merely slower movement during gait, but a fundamental disruption in the dynamic regulation of locomotor kinetics and rhythmic automaticity [47]. It also aligns with prior evidence that temporal variability is a sensitive marker of PD gait dysfunction and is associated with impaired basal ganglia contributions to rhythmic motor control [46,48,49].

Bilateral stride time variability was elevated in the PD group independent of mean stride time, indicating that the disease disrupts temporal consistency rather than the average pace of locomotion. This temporal instability has a well-characterized neurochemical basis: nigrostriatal dopaminergic degeneration impairs basal ganglia-thalamocortical modulation of locomotor timing and disrupts gait automaticity [50–52]. In PD, basal ganglia dysfunction disrupts the automatization of locomotor programs, compelling reliance on conscious cognitive control during walking that introduces attentional lapses and incomplete rhythmic programming, manifesting as increased stride-to-stride variability [53]. These findings indicate stride time variability is a candidate quantitative gait indicator related to fall risk stratification and treatment monitoring [11,54], rather than a stand-alone diagnostic marker.

Shortening swing-phase duration in both limbs, alongside prolonged right-sided stance time, reflects a systematic gait-cycle reorganization in PD, characterized by a distal-to-proximal shift in neuromuscular strategy: reduced ankle plantar flexor drive constrains push-off while proximal quadriceps and hamstring activation provide compensatory knee stabilization [55]. This propulsive deficit is directly reflected in the reduction in bilateral AP COP dispersion in the PD group, which indexes a constrained heel-to-toe transfer of body weight driven by impaired plantar flexor function—muscles that generate approximately 50% of stance-phase mechanical power in the lower extremity [56,57]. And this reduction is mechanically accompanied by an increase in compensatory work demands at proximal joints [58]. In contrast, preservation of mediolateral COP path dispersion suggests intact hip-abductor control of lateral balance, consistent with stage-dependent progression of PD motor deficits at mild to moderate Hoehn and Yahr stages. Together, this directional dissociation positions AP COP dispersion as a candidate biomarker for monitoring propulsive decline across disease stages in future longitudinal studies.

Elevation of the forefoot-to-rearfoot loading ratio on both sides reflects an anteriorly shifted plantar pressure distribution in PD, driven by the forward-flexed trunk posture that displaces the whole-body center of mass (COM) anteriorly, thereby increasing metatarsal loading while reducing heel contact pressure. This is consistent with prior literature showing that the degree of forefoot loading correlates with disease severity [59]. Axial rigidity constrains lumbar extension and promotes a fixed-flexion trunk posture [60–62], while disrupted basal ganglia output undermines the automatic postural adjustments that would ordinarily preserve upright alignment during locomotion [63,64]. Moreover, the right-side forefoot-to-rearfoot loading ratio emerged as the most influential gait-derived feature in the SHAP analysis, supporting its consideration as a core biomechanical discriminator of PD.

Significant inter-limb asymmetry in COP path length indicates that the spatial trajectory of weight transfer during stance is more sensitive to PD-related impairment than temporal or scalar force measures, likely because it integrates the full complexity of stance-phase neuromechanics across both the anteroposterior and mediolateral axes, rendering it a composite representative indicator for propulsive and balance control asymmetry between limbs. These findings support evaluating COP path asymmetry in future longitudinal and protocol-unified studies, while avoiding its interpretation as a validated prodromal or progression biomarker at this stage.

Statistical parametric mapping of stance-phase VGRF waveforms identified bilateral group differences in early and late stance, with an additional mid-stance difference on the right limb. Reduced early stance VGRF is consistent with a flat-foot or forefoot contact pattern and diminished tibialis anterior contribution at initial contact. Reduced late-stance loading indicates compromised plantar-flexor push-off, consistent with the constrained AP COP dispersion described above. The additional mid-stance difference on the right limb may reflect asymmetric weight-bearing strategies that redistribute loading between limbs.

The biomechanical alterations identified in this study should be interpreted as candidate indicators rather than validated clinical tools. Elevated bilateral stride-time variability indexes disrupted basal ganglia rhythmic control and have established links to fall risk, plausibly augmenting clinical fall-risk screening. Reduced anteroposterior COP dispersion reflects constrained heel-to-toe weight transfer and impaired ankle push-off and may serve as an early indicator of propulsive decline. Bilateral elevated forefoot-to-rearfoot loading ratio reflects the anteriorly displaced trunk posture characteristic of PD and could complement existing posture-based clinical assessments. Finally, the COP path symmetry index captures lateralized neuromechanical impairment, consistent with asymmetric dopaminergic degeneration.

The high participant-wise classification performance (AUC = 0.992) is consistent with prior machine learning studies using the same PhysioNet dataset [18,20,65,66]. Importantly, this result was achieved under strict participant-wise holdout partitioning, which prevents the performance inflation that arises when stride- or session-level observations from the same individual are distributed across training and test splits, an approach not consistently applied in prior work [67]. However, SHAP analysis identified clinical severity indicators, including UPDRS, UPDRSM, and Hoehn and Yahr stage, as the primary drivers of model predictions, with biomechanical gait features contributing as secondary determinants of classification. This reflects the strong covariance between disease severity and gait biomechanics in the dataset. Multimodal machine learning frameworks combining clinical severity with sensor-derived features routinely outperform single-modality gait models in PD [68,69]. Additionally, the forefoot-to-rearfoot loading ratio ranked as the most influential gait-derived feature in the SHAP analysis, independently corroborating the bilateral forefoot loading elevation observed in the group comparisons and reinforcing its role as a core biomechanical discriminator of PD in this dataset.

The contrast between the high within-protocol classification performance (AUC = 0.992) and the wide leave-one-study-out range (AUC: 0.500–1.000) is the central methodological finding of this study and should be acknowledged as the principal limitation of the analysis pipeline. The collapse to near-chance performance when the treadmill subset (Si) was held out demonstrates a well-recognized but rarely quantified limitation: feature distributions derived from one testing protocol may not generalize to other walking conditions. This reflects the absence of standardized PD gait testing protocols and unified digital gait biomarkers [16]. Consequently, a substantial portion of the discriminative signal captured by the model is dataset-specific rather than disease-specific, and reflects acquisition conditions (treadmill versus overground walking, dual-task versus single-task, rhythmic auditory cues) rather than a generalizable Parkinsonian gait signature. Accordingly, the high participant-wise holdout AUC cannot be taken as evidence of demonstrated generalizability, which requires explicit cross-protocol and external validation before any deployment claim can be substantiated.

The treadmill collapse is itself biomechanically meaningful: belt-fixed speed compresses the natural variation in walking speed that overground gait permits, narrowing the in-shoe feature distribution, and treadmill ambulation can act as an external pacemaker that transiently stabilizes PD gait rhythm. Mitigating these effects will require unified, protocol-harmonized acquisition standards across participating sites, explicit modeling of protocol as a covariate, domain-adversarial training to suppress protocol-discriminative representations, and prospective multi-site replication using a common minimal feature set so that protocol-invariance can be evaluated directly rather than inferred. Until externally validated across heterogeneous acquisition protocols, the present headline AUC describes within-dataset separability rather than clinical-grade transferability.

Although the leave-one-study-out AUC range (0.500–1.000) is wide and limits any single multivariable summary of model performance, the underlying univariate biomechanical findings include at least one indicator that behaves consistently across the cohort. Anteroposterior COP dispersion (COP_AP_SD) shows the largest standardized effect size among the kinetic features evaluated (bilateral Hedges' $|g| \approx 0.940$–1.120), remained significant after FDR correction on both limbs ($p < 0.001$), and demonstrated consistent directional effects bilaterally. Mechanistically, reduced COP_AP_SD reflects constrained heel-to-toe weight transfer consistent with impaired ankle push-off, and it also emerged as a principal gait-derived contributor in the SHAP analysis. On this basis, we identify COP_AP_SD as the most consistent single biomechanical indicator in the present cohort and prioritize it for prospective, protocol-unified validation as a candidate continu-

ous gait biomarker, alongside the forefoot-to-rearfoot loading ratio as a complementary moderate-to-large-effect indicator.

The gait-only sensitivity analysis quantified the discriminative contribution of biomechanical wearable-gait features in isolation by removing the clinical severity variables (UPDRS, UPDRSM, Hoehn and Yahr) and the TUAG functional mobility score from the feature matrix prior to the participant-wise split. Held-out performance fell substantially relative to the full multimodal model (gait-only AUC = 0.844 versus multimodal AUC = 0.992), and the residual discriminative signal in the selected gait-only model (SVM-RBF, in place of the HistGradientBoosting model selected by the primary analysis) was carried predominantly by bilateral anteroposterior COP dispersion (COP_AP_SD_L and COP_AP_SD_R), walking speed, and the COP path symmetry index (SI_COP_Path), anchoring the gait-only model in the same COP-derived measures that show the largest univariate effect sizes in the group-comparison analysis (Hedges' $|g| \approx 0.940$–1.120 for COP_AP_SD). Under leave-one-study-out evaluation, the dominant failure subset shifted from Si (treadmill) in the primary multimodal analysis to Ju (rhythmic auditory stimulation) in the gait-only analysis, consistent with auditory cueing normalizing PD timing variability and compressing the gait-derived discriminative signal between groups, and indicating that the treadmill-specific failure of the primary model was at least partly driven by protocol-correlated heterogeneity in the clinical severity variables rather than by an in-shoe sensor limitation. Together, these findings indicate that the high AUC of the primary multimodal classifier is attributable in substantial part to the inclusion of clinical severity variables rather than to the wearable-gait signal alone, and that advancing toward a standalone gait biomarker will require either feature-engineering strategies that isolate gait signatures from disease-severity covariance, or a shift in clinical objective from binary PD classification toward targeted biomechanical tracking of functionally relevant motor impairments such as AP COP dispersion and the forefoot-to-rearfoot loading ratio, which represent promising candidates for prospective, multi-cohort validation.

Several limitations should be acknowledged. The SPM waveform analysis was conducted on trial-level mean waveforms rather than participant-averaged waveforms, meaning that participants with multiple recording sessions contributed more than one observation and strict statistical independence at the participant-level cannot be guaranteed; waveform findings should therefore be interpreted with appropriate caution. The cohort represented predominantly mild-to-moderate disease severity (Hoehn and Yahr 2.0–3.0), limiting generalization to advanced PD or individuals with freezing gait. Walking was performed under controlled, unobstructed conditions, which may not reflect the more complex demands of real-world ambulation. Finally, the cross-sectional design precludes any assessment of whether the identified biomechanical features track disease progression or respond to therapeutic intervention longitudinally.

5. Conclusions

This study provides a mechanistically grounded characterization of Parkinsonian gait impairment, demonstrating that the disease signature encompasses striatal dopaminergic timing instability reflected in elevated stride time variability, impaired propulsive foot-ground mechanics reflected in constrained AP COP dispersion and forefoot loading dominance, and lateralized neuromechanical asymmetry reflected in elevated COP path asymmetry. The kinetic and COP-derived measures yielded consistently larger effect sizes than conventional spatiotemporal parameters, identifying them as candidate targets for future biomarker development. Machine learning classification achieved high within-protocol performance but exposed substantial cross-protocol heterogeneity (AUC range 0.500–1.000), which we acknowledge as the central limitation of the present analysis,

and SHAP analysis confirmed that model predictions were driven by multimodal disease severity rather than gait-derived wearable features alone. The work therefore presents a structured, interpretable analysis pipeline rather than a fully established framework for digital biomarker development. A pre-specified gait-only sensitivity analysis, which removed clinical severity variables from the feature set, further confirmed that biomechanical wearable-gait features alone retained only moderate, substantially reduced discriminative ability (gait-only holdout AUC = 0.844) and exhibited protocol-dependent collapse on a different subset (Ju rather than Si) than the primary multimodal model, reinforcing that the headline classification performance reflects multimodal clinical separation rather than a stand-alone wearable-gait biomarker. External validation in independent cohorts and prospective testing across acquisition protocols are required before clinical translation can be claimed. Future work should prioritize longitudinal validation of AP COP dispersion and forefoot-to-rearfoot loading ratio as disease-tracking biomarkers, protocol-unified multi-site replication, and the development of gait-specific classification approaches that are explicitly independent of clinical severity ratings, enabling genuine standalone wearable sensor-based PD assessment.

Funding: This research was funded by the College of Health and Human Sciences at San José State University under a College Unrestricted Research Fund award.

Institutional Review Board Statement: Not applicable.

Informed Consent Statement: Not applicable.

Data Availability Statement: The data presented in this study are available in Goldberger et al. [17]. The data presented in this study were derived from the following resources available in the public domain: [Available online: https://physionet.org/content/gaitpdb/1.0.0/ (accessed on 1 December 2025)].

Acknowledgments: Research reported in this publication was supported by the College of Health and Human Sciences at San José State University under a College Unrestricted Research Fund award. The content is solely the responsibility of the author and does not necessarily represent the official views of San José State University.

Conflicts of Interest: The author declares no conflicts of interest.

References

1. Luo, Y.; Qiao, L.; Li, M.; Wen, X.; Zhang, W.; Li, X. Global, Regional, National Epidemiology and Trends of Parkinson's Disease from 1990 to 2021: Findings from the Global Burden of Disease Study 2021. *Front. Aging Neurosci.* **2024**, *16*, 1498756. [CrossRef] [PubMed]
2. Su, D.; Cui, Y.; He, C.; Yin, P.; Bai, R.; Zhu, J.; Lam, J.S.T.; Zhang, J.; Yan, R.; Zheng, X.; et al. Projections for Prevalence of Parkinson's Disease and Its Driving Factors in 195 Countries and Territories to 2050: Modelling Study of Global Burden of Disease Study 2021. *BMJ* **2025**, *388*, e080952. [CrossRef] [PubMed]
3. Mirelman, A.; Bonato, P.; Camicioli, R.; Ellis, T.D.; Giladi, N.; Hamilton, J.L.; Hass, C.J.; Hausdorff, J.M.; Pelosin, E.; Almeida, Q.J. Gait Impairments in Parkinson's Disease. *Lancet Neurol.* **2019**, *18*, 697–708. [CrossRef] [PubMed]
4. Ben-Shlomo, Y.; Darweesh, S.; Llibre-Guerra, J.; Marras, C.; San Luciano, M.; Tanner, C. The Epidemiology of Parkinson's Disease. *Lancet* **2024**, *403*, 283–292. [CrossRef] [PubMed]
5. Morris, M.E.; Huxham, F.; McGinley, J.; Dodd, K.; Iansek, R. The Biomechanics and Motor Control of Gait in Parkinson Disease. *Clin. Biomech.* **2001**, *16*, 459–470. [CrossRef] [PubMed]
6. Bonacina, D.; Tosatto, D.; Ugolini, A.; Rossi, F.; Corno, I.; Pellicciari, L.; Perin, C.; Colón-Semenza, C.; Piscitelli, D. Spatiotemporal, Kinematic and Kinetic Gait Characteristics in Parkinson's Disease Compared to Healthy Individuals: A Systematic Review with Meta-Analysis. *Clin. Biomech.* **2024**, *120*, 106359. [CrossRef]
7. Hausdorff, J.M.; Cudkowicz, M.E.; Firtion, R.; Wei, J.Y.; Goldberger, A.L. Gait Variability and Basal Ganglia Disorders: Stride-to-Stride Variations of Gait Cycle Timing in Parkinson's Disease and Huntington's Disease. *Mov. Disord.* **1998**, *13*, 428–437. [CrossRef] [PubMed]
8. Allen, N.E.; Schwarzel, A.K.; Canning, C.G. Recurrent Falls in Parkinson's Disease: A Systematic Review. *Park. Dis.* **2013**, *2013*, 906274. [CrossRef] [PubMed]

9. Creaby, M.W.; Cole, M.H. Gait Characteristics and Falls in Parkinson's Disease: A Systematic Review and Meta-Analysis. *Park. Relat. Disord.* **2018**, *57*, 1–8. [CrossRef] [PubMed]
10. Schmitt, A.C.; Baudendistel, S.T.; Fallon, M.S.; Roper, J.A.; Hass, C.J. Assessing the Relationship between the Enhanced Gait Variability Index and Falls in Individuals with Parkinson's Disease. *Park. Dis.* **2020**, *2020*, 5813049. [CrossRef] [PubMed]
11. Ma, L.; Mi, T.M.; Jia, Q.; Han, C.; Chhetri, J.K.; Chan, P. Gait Variability Is Sensitive to Detect Parkinson's Disease Patients at High Fall Risk. *Int. J. Neurosci.* **2022**, *132*, 888–893. [CrossRef] [PubMed]
12. Plotnik, M.; Giladi, N.; Hausdorff, J.M. A New Measure for Quantifying the Bilateral Coordination of Human Gait: Effects of Aging and Parkinson's Disease. *Exp. Brain Res.* **2007**, *181*, 561–570. [CrossRef] [PubMed]
13. Silveira-Ciola, A.P.; Seuthe, J.; Coelho, D.B.; Faria, M.H.; Santinelli, F.B.; Schlenstedt, C.; Barbieri, F.A. Gait Asymmetry in Parkinson's Disease—A Systematic Review and Meta-Analysis (AsymmGait-Parkinson Study). *Sci. Rep.* **2026**, *16*, 11682. [CrossRef] [PubMed]
14. Patoz, A.; Malatesta, D.; Burtscher, J. Isolating the Speed Factor Is Crucial in Gait Analysis for Parkinson's Disease. *Front. Neurosci.* **2023**, *17*, 1119390. [CrossRef] [PubMed]
15. Giannakou, E.; Fotiadou, S.; Gourgoulis, V.; Mavrommatis, G.; Aggelousis, N. A Comparative Analysis of Symmetry Indices for Spatiotemporal Gait Features in Early Parkinson's Disease. *Neurol. Int.* **2023**, *15*, 1129–1139. [CrossRef] [PubMed]
16. Mancini, M.; Afshari, M.; Almeida, Q.; Amundsen-Huffmaster, S.; Balfany, K.; Camicioli, R.; Christiansen, C.; Dale, M.L.; Dibble, L.E.; Earhart, G.M.; et al. Digital Gait Biomarkers in Parkinson's Disease: Susceptibility/Risk, Progression, Response to Exercise, and Prognosis. *npj Park. Dis.* **2025**, *11*, 51. [CrossRef]
17. Goldberger, A.L.; Amaral, L.A.; Glass, L.; Hausdorff, J.M.; Ivanov, P.C.; Mark, R.G.; Mietus, J.E.; Moody, G.B.; Peng, C.K.; Stanley, H.E. PhysioBank, PhysioToolkit, and PhysioNet: Components of a New Research Resource for Complex Physiologic Signals. *Circulation* **2000**, *101*, E215–E220. [CrossRef] [PubMed]
18. Navita; Mittal, P.; Sharma, Y.K.; Rai, A.K.; Simaiya, S.; Lilhore, U.K.; Kumar, V. Gait-Based Parkinson's Disease Diagnosis and Severity Classification Using Force Sensors and Machine Learning. *Sci. Rep.* **2025**, *15*, 328. [CrossRef] [PubMed]
19. Li, A.; Li, C. Detecting Parkinson's Disease through Gait Measures Using Machine Learning. *Diagnostics* **2022**, *12*, 2404. [CrossRef] [PubMed]
20. Balaji, E.; Brindha, D.; Balakrishnan, R. Supervised Machine Learning Based Gait Classification System for Early Detection and Stage Classification of Parkinson's Disease. *Appl. Soft Comput.* **2020**, *94*, 106494. [CrossRef]
21. Tahir, N.M.; Manap, H.H. Parkinson Disease Gait Classification Based on Machine Learning Approach. *J. Appl. Sci.* **2012**, *12*, 180–185. [CrossRef]
22. Camps, J.; Samà, A.; Martín, M.; Rodríguez-Martín, D.; Pérez-López, C.; Moreno Arostegui, J.M.; Cabestany, J.; Català, A.; Alcaine, S.; Mestre, B.; et al. Deep Learning for Freezing of Gait Detection in Parkinson's Disease Patients in Their Homes Using a Waist-Worn Inertial Measurement Unit. *Knowl.-Based Syst.* **2018**, *139*, 119–131. [CrossRef]
23. Diaz, M.; Ferrer, M.A.; Impedovo, D.; Pirlo, G.; Vessio, G. Dynamically Enhanced Static Handwriting Representation for Parkinson's Disease Detection. *Pattern Recognit. Lett.* **2019**, *128*, 204–210. [CrossRef]
24. Diaz, M.; Moetesum, M.; Siddiqi, I.; Vessio, G. Sequence-Based Dynamic Handwriting Analysis for Parkinson's Disease Detection with One-Dimensional Convolutions and BiGRUs. *Expert Syst. Appl.* **2021**, *168*, 114405. [CrossRef]
25. Lundberg, S.M.; Lee, S.-I. A Unified Approach to Interpreting Model Predictions. In *Proceedings of the 31st International Conference on Neural Information Processing Systems*; NIPS'17; Curran Associates Inc.: Long Beach, CA, USA, 2017; pp. 4768–4777. [CrossRef]
26. Yogev, G.; Giladi, N.; Peretz, C.; Springer, S.; Simon, E.S.; Hausdorff, J.M. Dual Tasking, Gait Rhythmicity, and Parkinson's Disease: Which Aspects of Gait Are Attention Demanding? *Eur. J. Neurosci.* **2005**, *22*, 1248–1256. [CrossRef] [PubMed]
27. Hausdorff, J.M.; Lowenthal, J.; Herman, T.; Gruendlinger, L.; Peretz, C.; Giladi, N. Rhythmic Auditory Stimulation Modulates Gait Variability in Parkinson's Disease. *Eur. J. Neurosci.* **2007**, *26*, 2369–2375. [CrossRef] [PubMed]
28. Frenkel-Toledo, S.; Giladi, N.; Peretz, C.; Herman, T.; Gruendlinger, L.; Hausdorff, J.M. Treadmill Walking as an External Pacemaker to Improve Gait Rhythm and Stability in Parkinson's Disease. *Mov. Disord.* **2005**, *20*, 1109–1114. [CrossRef] [PubMed]
29. Jiang, X.; Napier, C.; Hannigan, B.; Eng, J.J.; Menon, C. Estimating Vertical Ground Reaction Force during Walking Using a Single Inertial Sensor. *Sensors* **2020**, *20*, 4345. [CrossRef] [PubMed]
30. Schaafsma, J.D.; Giladi, N.; Balash, Y.; Bartels, A.L.; Gurevich, T.; Hausdorff, J.M. Gait Dynamics in Parkinson's Disease: Relationship to Parkinsonian Features, Falls and Response to Levodopa. *J. Neurol. Sci.* **2003**, *212*, 47–53. [CrossRef] [PubMed]
31. Hausdorff, J.M.; Lertratanakul, A.; Cudkowicz, M.E.; Peterson, A.L.; Kaliton, D.; Goldberger, A.L. Dynamic Markers of Altered Gait Rhythm in Amyotrophic Lateral Sclerosis. *J. Appl. Physiol.* **2000**, *88*, 2045–2053. [CrossRef] [PubMed]
32. Hausdorff, J.M.; Rios, D.A.; Edelberg, H.K. Gait Variability and Fall Risk in Community-Living Older Adults: A 1-Year Prospective Study. *Arch. Phys. Med. Rehabil.* **2001**, *82*, 1050–1056. [CrossRef] [PubMed]
33. Hausdorff, J.M.; Balash, J.; Giladi, N. Effects of Cognitive Challenge on Gait Variability in Patients with Parkinson's Disease. *J. Geriatr. Psychiatry Neurol.* **2003**, *16*, 53–58. [CrossRef] [PubMed]

34. Frenkel-Toledo, S.; Giladi, N.; Peretz, C.; Herman, T.; Gruendlinger, L.; Hausdorff, J.M. Effect of Gait Speed on Gait Rhythmicity in Parkinson's Disease: Variability of Stride Time and Swing Time Respond Differently. *J. Neuroeng. Rehabil.* **2005**, *2*, 23. [CrossRef] [PubMed]
35. Mittal, R.; Agarwal, N.; Dubey, M.; Pathak, V.; Shukla, P.; Rani, G.; Vocaturo, E.; Zumpano, E. Machine Learning Approach to Gait Analysis for Parkinson's Disease Detection and Severity Classification. *Front. Robot. AI* **2025**, *12*, 1623529. [CrossRef] [PubMed]
36. Robinson, R.O.; Herzog, W.; Nigg, B. Use of Force Platform Variables to Quantify the Effects of Chiropractic Manipulation on Gait Symmetry. *J. Manip. Physiol. Ther.* **1987**, *4*, 172–176. [PubMed]
37. Viteckova, S.; Kutilek, P.; Svoboda, Z.; Krupicka, R.; Kauler, J.; Szabo, Z. Gait Symmetry Measures: A Review of Current and Prospective Methods. *Biomed. Signal Process. Control* **2018**, *42*, 89–100. [CrossRef]
38. Queen, R.; Dickerson, L.; Ranganathan, S.; Schmitt, D. A Novel Method for Measuring Asymmetry in Kinematic and Kinetic Variables: The Normalized Symmetry Index. *J. Biomech.* **2020**, *99*, 109531. [CrossRef] [PubMed]
39. Pataky, T.C. Generalized N-Dimensional Biomechanical Field Analysis Using Statistical Parametric Mapping. *J. Biomech.* **2010**, *43*, 1976–1982. [CrossRef] [PubMed]
40. Breiman, L. Random Forests. *Mach. Learn.* **2001**, *45*, 5–32. [CrossRef]
41. Ke, G.; Meng, Q.; Finley, T.; Wang, T.; Chen, W.; Ma, W.; Ye, Q.; Liu, T.-Y. LightGBM: A Highly Efficient Gradient Boosting Decision Tree. In *Proceedings of the 31st International Conference on Neural Information Processing Systems*; NIPS'17; Curran Associates Inc.: Long Beach, CA, USA, 2017; pp. 3149–3157.
42. Friedman, J.H. Greedy Function Approximation: A Gradient Boosting Machine. *Ann. Stat.* **2001**, *29*, 1189–1232. [CrossRef]
43. Cortes, C.; Vapnik, V. Support-Vector Networks. *Mach. Learn.* **1995**, *20*, 273–297. [CrossRef]
44. Rumelhart, D.E.; Hinton, G.E.; Williams, R.J. Learning Representations by Back-Propagating Errors. *Nature* **1986**, *323*, 533–536. [CrossRef]
45. Pedregosa, F.; Varoquaux, G.; Gramfort, A.; Michel, V.; Thirion, B.; Blondel, M.; Müller, A.; Norhman, J.; Louppe, G.; Prettenhofer, P.; et al. Scikit-Learn: Machine Learning in Python. *J. Mach. Learn. Res.* **2011**, *12*, 2825–2830. [CrossRef]
46. Hausdorff, J.M.; Schaafsma, J.D.; Balash, Y.; Bartels, A.L.; Gurevich, T.; Giladi, N. Impaired Regulation of Stride Variability in Parkinson's Disease Subjects with Freezing of Gait. *Exp. Brain Res.* **2003**, *149*, 187–194. [CrossRef] [PubMed]
47. Takakusaki, K. Functional Neuroanatomy for Posture and Gait Control. *J. Mov. Disord.* **2017**, *10*, 1–17. [CrossRef] [PubMed]
48. Hausdorff, J.M. Gait Variability: Methods, Modeling and Meaning. *J. Neuroeng. Rehabil.* **2005**, *2*, 19. [CrossRef] [PubMed]
49. Snijders, A.H.; van de Warrenburg, B.P.; Giladi, N.; Bloem, B.R. Neurological Gait Disorders in Elderly People: Clinical Approach and Classification. *Lancet Neurol.* **2007**, *6*, 63–74. [CrossRef] [PubMed]
50. Almeida, Q.J.; Frank, J.S.; Roy, E.A.; Patla, A.E.; Jog, M.S. Dopaminergic Modulation of Timing Control and Variability in the Gait of Parkinson's Disease. *Mov. Disord.* **2007**, *22*, 1735–1742. [CrossRef] [PubMed]
51. Galvan, A.; Devergnas, A.; Wichmann, T. Alterations in Neuronal Activity in Basal Ganglia-Thalamocortical Circuits in the Parkinsonian State. *Front. Neuroanat.* **2015**, *9*, 5. [CrossRef] [PubMed]
52. Surmeier, D.J.; Graves, S.M.; Shen, W. Dopaminergic Modulation of Striatal Networks in Health and Parkinson's Disease. *Curr. Opin. Neurobiol.* **2014**, *29*, 109–117. [CrossRef] [PubMed]
53. Wu, T.; Hallett, M.; Chan, P. Motor Automaticity in Parkinson's Disease. *Neurobiol. Dis.* **2015**, *82*, 226–234. [CrossRef] [PubMed]
54. König, N.; Singh, N.B.; Baumann, C.R.; Taylo, W.R. Can Gait Signatures Provide Quantitative Measures for Aiding Clinical Decision-Making? A Systematic Meta-Analysis of Gait Variability Behavior in Patients with Parkinson's Disease. *Front. Hum. Neurosci.* **2016**, *10*, 319. [CrossRef] [PubMed]
55. Islam, A.; Alcock, L.; Nazarpour, K.; Rochester, L.; Pantall, A. Effect of Parkinson's Disease and Two Therapeutic Interventions on Muscle Activity during Walking: A Systematic Review. *npj Park. Dis.* **2020**, *6*, 22. [CrossRef] [PubMed]
56. Jin, L.; Hahn, M.E. Modulation of Lower Extremity Joint Stiffness, Work and Power at Different Walking and Running Speeds. *Hum. Mov. Sci.* **2018**, *58*, 1–9. [CrossRef] [PubMed]
57. Jin, L.; Hahn, M.E. Comparison of Lower Extremity Joint Mechanics between Healthy Active Young and Middle Age People in Walking and Running Gait. *Sci. Rep.* **2019**, *9*, 5568. [CrossRef] [PubMed]
58. Fickey, S.N.; Browne, M.G.; Franz, J.R. Biomechanical Effects of Augmented Ankle Power Output during Human Walking. *J. Exp. Biol.* **2018**, *221*, jeb182113. [CrossRef] [PubMed]
59. Stolze, H.; Kuhtz-Buschbeck, J.P.; Drücke, H.; Jöhnk, K.; Illert, M.; Deuschl, G. Comparative Analysis of the Gait Disorder of Normal Pressure Hydrocephalus and Parkinson's Disease. *J. Neurol. Neurosurg. Psychiatry* **2001**, *70*, 289–297. [CrossRef] [PubMed]
60. Wright, W.G.; Gurfinkel, V.S.; Nutt, J.; Horak, F.B.; Cordo, P.J. Axial Hypertonicity in Parkinson's Disease: Direct Measurements of Trunk and Hip Torque. *Exp. Neurol.* **2007**, *208*, 38. [CrossRef] [PubMed]
61. Cano-De-la-Cuerda, R.; Vela-Desojo, L.; Moreno-Verdú, M.; Ferreira-Sánchez, M.D.R.; Macías-Macías, Y.; Miangolarra-Page, J.C. Trunk Range of Motion Is Related to Axial Rigidity, Functional Mobility and Quality of Life in Parkinson's Disease: An Exploratory Study. *Sensors* **2020**, *20*, 2482. [CrossRef] [PubMed]

62. Geroin, C.; Artusi, C.A.; Nonnekes, J.; Aquino, C.; Garg, D.; Dale, M.L.; Schlosser, D.; Lai, Y.; Al-Wardat, M.; Salari, M.; et al. Axial Postural Abnormalities in Parkinsonism: Gaps in Predictors, Pathophysiology, and Management. *Mov. Disord.* **2023**, *38*, 732–739. [CrossRef] [PubMed]
63. Peterson, D.S.; Horak, F.B. Neural Control of Walking in People with Parkinsonism. *Physiology* **2016**, *31*, 95. [CrossRef] [PubMed]
64. Park, J.-H.; Kang, Y.-J.; Horak, F.B. What Is Wrong with Balance in Parkinson's Disease? *J. Mov. Disord.* **2015**, *8*, 109. [CrossRef] [PubMed]
65. El Maachi, I.; Bilodeau, G.A.; Bouachir, W. Deep 1D-Convnet for Accurate Parkinson Disease Detection and Severity Prediction from Gait. *Expert. Syst. Appl.* **2020**, *143*, 113075. [CrossRef]
66. Balaji, E.; Brindha, D.; Umesh, K. Data-Driven Gait Analysis for Diagnosis and Severity Rating of Parkinson's Disease. *Med. Eng. Phys.* **2021**, *91*, 54–64. [CrossRef]
67. Starcke, J.; Spadafora, J.; Spadafora, J.; Spadafora, P.; Toma, M. The Effect of Data Leakage and Feature Selection on Machine Learning Performance for Early Parkinson's Disease Detection. *Bioengineering* **2025**, *12*, 845. [CrossRef] [PubMed]
68. Brzenczek, C.; Klopfenstein, Q.; Hähnel, T.; Fröhlich, H.; Glaab, E.; Zelimkhanov, G.; Wollscheid-Lengeling, E.; Wilmes, P.; Vilas Boas, L.; Vega, C.; et al. Integrating Digital Gait Data with Metabolomics and Clinical Data to Predict Outcomes in Parkinson's Disease. *npj Digit. Med.* **2024**, *7*, 235. [CrossRef] [PubMed]
69. Ravichandran, A.; Kathirvel Murugan, T.; Govindaraj, L.; M, V. Explainable Multimodal Feature Fusion Networks for Parkinson's Disease Prediction. *Front. Digit. Health* **2026**, *8*, 1771281. [CrossRef] [PubMed]

Disclaimer/Publisher's Note: The statements, opinions and data contained in all publications are solely those of the individual author(s) and contributor(s) and not of MDPI and/or the editor(s). MDPI and/or the editor(s) disclaim responsibility for any injury to people or property resulting from any ideas, methods, instructions or products referred to in the content.